Is there a common drive for buccal movements associated with buccal and lung 'breath' in Lithobates catesbeianus?

Brigitte Quenet, Ginette Horcholle-Bossavit, Stéphanie Fournier, Tara Adele Janes, Richard Kinkead

Available online at www.sciencedirect.com
ScienceDirect
Respiratory Physiology & Neurobiology (2019) –10
RPN

Is there a common drive for buccal movements associated with buccal and lung 'breath' in *Lithobates catesbeianus* ?

Brigitte Quenet[1,2], Ginette Horcholle-Bossavit[1,2], Stéphanie Fournier[3], Tara Adele Janes[3], Richard Kinkead[3]

[1] *PSL Research University, ESPCI-Paris*
Équipe de Statistique Appliquée, F-75005 Paris, France
Tel.: +133-40-794461

[2] *Sorbonne Université, INSERM, UMRS1158 Neurophysiologie respiratoire expérimentale et clinique, F-75013 Paris, France*

[3] *Department of Pediatrics, Université Laval*
Institut Universitaire de Cardiologie et de Pneumologie de Québec (IUCPQ), Québec, Canada

Abstract

In amphibians, there is some evidence that (1) anatomically separate brainstem respiratory oscillators are involved in rhythm generation, one for the buccal rhythm and another for the lung rhythm and (2) they become functionally coupled during metamorphosis. The present analysis, performed on neurograms recorded using brainstem preparations from *Lithobates catesbeianus*, aims to investigate the temporal organisation of lung and buccal burst types. Continuous Wavelet Transfom applied to the separated buccal and lung signals of a neurogram revealed that both buccal and lung frequency profiles exhibited the same low frequency peak around 1 Hz. This suggests that a common 'clock' organises both rhythms within an animal. A cross-correlation analysis applied to the buccal and lung burst signals revealed their similar intrinsic oscillation features, occurring at approximately 25 Hz. These observations suggest that a coupling between the lung and buccal oscillators emerges at metamorphosis. This coupling may be related to inter-connectivity between the two oscillators, and to a putative common drive.

Keywords: Frog ventilation, Buccal and lung fast oscillations, Ventilatory CPG drive, Buccal and lung coupling, cross-correlation coefficients

1. Introduction

In amphibians, respiratory gas exchange occurs in several locations (skin, gills and lungs), and the relative contribution of each respiratory surface changes with development (Burggren & West (1982)). The first developmental stages of amphibians are aquatic, and gas exchange (O_2 and CO_2) is performed through the skin and gills (Sundin et al. (2007)). Pre-metamorphic tadpoles ventilate the gills by rhythmic contractions of the buccal musculature, which moves the buccal floor up and down, causing water to flow over the gills. This buccal pump is driven by a neuronal command thought to originate from a Central Pattern Generator (CPG) producing the low-amplitude buccal motor activity. As the animal metamorphoses into an adult frog, the gills regress and the lungs develop the capacity for effective oxygen uptake. In the adult American bullfrog *Lithobates catesbeianus*, several types of movements associated with air breathing are observed (Vitalis & Shelton (1990)). The first are oscillations of the buccal floor which, when combined with open nares, allows air movement in and out of the buccal cavity. These buccal oscillations are

Email address: Brigitte.Quenet@espci.fr (Brigitte Quenet)

interrupted periodically by a second type of more forceful contraction facilitating lung ventilation. For inspiration, the nares close, the glottis opens, and compression of the buccal floor forces air into the lungs by positive pressure. Expiration occurs when the glottis and nares are opened and the lungs passively deflate, allowing air to pass into the expanded buccal cavity and through the open nares. Next, the glottis closes, the nares remain open, and the buccal oscillations resume allowing residual air from the lungs to mix with fresh air drawn in through the nares. These buccal oscillations also bring air into contact with the nasal epithelium and are thought to contribute to olfaction (Gans et al. (1969), West & Jones (1975b,a), MacIntyre & Toews (1976), Jones (1982)). Many investigations into neural control of breathing have utilised isolated brainstems derived from *L. catesbeianus* because the motor output from these preparations (recorded via the cranial nerves, CNs) corresponds very well with the ventilatory movements observed in intact tadpoles and frogs (Sakakibara (1984a,b), Kogo et al. (1994), Kogo & Remmers (1994), McLean et al. (1995), Torgerson et al. (1997), Gdovin et al. (1998, 1999), Wilson et al. (1999), Santin & Hartzler (2016)). Indeed, the motor activity recorded from CNs V, VII, X, and spinal nerve II exhibits regular low-amplitude bursts associated with gill ventilation in pre-metamorphic tadpoles and episodic, high-amplitude bursts corresponding to lung ventilation in post-metamorphic tadpoles and adult frogs (Galante et al. (1996)). In addition to the regular buccal activity observed for pre-metamorphic tadpoles, spontaneous expression of a neuronal command for lung ventilation is observable, but occurs infrequently (Galante et al. (1996), Duchcherer et al. (2013)). After metamorphosis, the expression of the neuronal command for lung ventilation becomes more frequent (Taylor et al. (2003a,b)) concurrent with increased reliance on air breathing for gas exchange. Several studies indicate that the buccal and lung motor commands arise from at least two distinct oscillators, potentially three (Wilson et al. (2002), Baghdadwala et al. (2015)). It has been suggested that the lung oscillator has a rostral position in the medulla, while the buccal oscillator is located in the caudal medulla (Vasilakos et al. (2006), Duchcherer et al. (2013)). Other studies using optical monitoring of brainstem neurons revealed that rhythmic activity correlated to the ventilatory cycle was exhibited by a rostro-caudal column of neurons located within the ventrolateral medulla between the levels of the trigeminal and hypoglossal rootlets (Oku et al. (2008)). In mammals, the existence of two respiratory oscillators has been well characterised in rats (Feldman & DelNegro (2006), DelNegro et al. (2018)). These oscillators are associated with two brainstem nuclei, the Parafacial Respiratory Group (pFRG) and the Pre-Bötzinger Complex (pre-BotC) (Smith et al. (1991), Onimaru & Homma (2003)). It has been proposed that these oscillators may have originated from those controlling the gills and lungs of the earliest air breathers (Wilson et al. (1999)), although this remains to be demonstrated experimentally. The motoneurons innervating the respiratory muscles are recruited by premotor neurons, whose activity is driven by both the buccal and lung oscillators; thus, motoneuron activity, which can be recorded from the CNs, reflects the descending oscillator command. Analyses of the timing of the gill and lung bursts recorded as neurograms show that these oscillators, if distinct, are functionally coupled in the post-metamorphic animal (Trask et al. (2018)). With that in mind, the objective of the present study was to re-evaluate this concept using a different approach. Specifically, we analysed filtered neurograms using the signal processing tools previously applied to for the analysis of *Pelophylax ridibundus* respiratory motor patterns (Quenet et al. (2014)). The tools utilised by Quenet et al. (2014), which are based on Continuous Wavelet Transform (CWT) and cross-correlation analyses, were used to analyse the buccal activity only, and provided proof-of-principle for the current methodology. The main results of this study on *P. ridibundus* revealed the presence of a temporal grid inside all buccal bursts in pre-metamorphic and post-metamorphic tadpole recordings. This buccal temporal grid emerges as fast oscillations (20-25 Hz) of the mean buccal burst amplitude profile, whatever the value of the fundamental frequency of the buccal rhythm. This buccal temporal grid is revealed by fast oscillations (20-25 Hz) of the mean buccal burst amplitude profile, whatever the value of the fundamental frequency of buccal rhythm. The present analysis, using neurograms recorded from *L. catesbeianus* pre- and post-metamorphic tadpoles, and adult brainstem preparations indicates that the buccal bursts exhibit fast oscillations in the 15-35 Hz frequency range, which encompasses the range of observed frequencies in *P. ridibundus*. In the present study, the analysis of the lung bursts reveals that they also exhibit a temporal grid with fast oscillations similar to that of the buccal bursts in the same neurogram.

2. Materials and Methods

2.1. Data collection

2.1.1. Isolated Brainstem Preparations

Experiments were performed using pre-metamorphic (TK stages VI-XII) and post-metamorphic *L. catesbeianus* tadpoles (TK stages XXIII-XXIV), and adult frogs (sexually mature). Animals were obtained from a commercial supplier (Island Bullfrog, Nanaimo, BC, Canada) and housed in aquaria containing flowing, filtered and de-chlorinated Québec City water at 19-22°C. All experiments complied with the guidelines of the Canadian Council on Animal Care and were approved by the institutional animal care committee. Isolated brainstem preparations were made as previously described (Fournier et al. (2007)). Briefly, animals were anesthetised (MS-222, 0.06g l-1) and the cranium opened to permit dissection of the brainstem and CNs. During dissection, neural tissue was irrigated continuously with cold (0-5 C) artificial cerebrospinal fluid (aCSF) prepared as follows: (in mM): for pre-metamorphic tadpoles: 90 NaCl, 4 KCl, 1.4 $MgCl_2$, 2.4 $CaCl_2$, 25 $NaHCO_3$, 1 NaH_2PO_4 7.5 D-glucose; for post-metamorphic tadpoles and adults: 75 NaCl, 4.5 KCl, 1 $MgCl_2$, 2.5 $CaCl_2$, 40 $NaHCO_3$, 1 NaH_2PO_4 7.5 D-glucose (Sigma Aldrich). The aCSF for pre-metamorphic tadpoles was equilibrated with a mixture of 1.8% CO_2 + 98.2% O_2 to pH 7.90 0.05, while that for post-metamorphic tadpoles and adults was equilibrated with 2.5% CO_2 + 97.5% O_2 to pH 7.80 0.15.

2.1.2. Electrophysiological Recordings

Brainstem preparations recovered for 40 mins in oxygenated aCSF (1.8% CO_2 + 98.2% O_2) before experiments commenced. Bursts of respiratory-related motor activity were recorded simultaneously from CNs V and X using suction electrodes constructed from borosilicate glass (0.84 mm i.d.; Stoelting Instrument vertical microelectrode puller, USA). Neural signals were amplified (gain = 10,000) and filtered (low cut-off: 10 Hz; high cut-off: 1 kHz) using a differential AC amplifier (model 1700; AM systems, USA). Resulting signals were digitized using a DI-720 data acquisition system at a conversion of 2500 Hz (Dataq Instruments, USA). Once a stable neural signal was achieved, 20 mins of baseline activity was recorded during perfusion with oxygenated aCSF. The perfusion was then switched to aCSF equilibrated with either a hypoxic gas mixture (1.8% CO_2 + 98.2% N_2; pH 7.9 ± 0.15) or hypercapnia (5% CO_2 + 95% O_2; pH 7.33 ± 0.04), for 20 mins. We have previously shown that the respiratory motor rhythm of tadpoles is chemoresponsive to hypoxia, while adults respond to hypercapnia. These data informed our decision to use a hypoxic perfusate for tadpoles and a hypercapnic perfusate for adults. Note that in previous experiments, we used an oxygen micro-electrode (MI-730; Microelectrodes Inc. NH, USA) to determine the definite oxygen level within the recording chamber resulting from the mixing of room air with the hypoxic perfusate; this was typically 5-7% O_2. All solutions were maintained at room temperature (21-23°C).

2.2. Trigeminal Neurogram processing

Recordings were obtained for the present study from a total of 21 *Lithobates catesbeianus* preparations. From these, we selected only those preparations that yielded neurograms that met the conditions of our analysis, giving us a final total of 6 pre-metamorphic tadpole preparations (two at stage VI, two at stage X and two at stage XII), 2 from post-metamorphic tadpoles and 2 from adult frogs. Two neurograms of five mins duration were obtained from each preparation: one during baseline conditions and a second during stimulated conditions (hypoxia or hypercapnia). All the signals were resampled at 2000 Hz. Frequency and amplitude processing tools were individually applied to each neurogram. Neurograms of 5 mins duration contained sufficient buccal bursts to provide an adequate representation of the typical features of the buccal activity. In order to accurately characterise the lung bursts (which are usually less numerous than the buccal bursts) and compare them to the buccal bursts within the same recording, we analysed only those recordings exhibiting a lung burst frequency that was >10% of the total respiratory activity. Using this criterion, we selected 8 neurograms (two per animal as stated above) originating from two post-metamorphic tadpoles and two adult frogs.

2.2.1. Separation of the buccal and lung bursts of each filtered neurogram and building corresponding separated buccal and lung signals

Each neurogram (illustrated in gray in Fig. 1A) was filtered using a zero-phase moving root mean square (RMS) with a rectangular window of width W = 200 ms or W = 10 ms, producing an S_{200} signal (black) and S_{10} signal

(red), respectively. The resulting S_{200} signal is an integrated representation of the neurogram, where each maximum corresponds to a burst within a cycle and each minimum (between two maxima) defines the transition between two successive cycles. On the S_{200} signal, an automatic detection of the successive minima was performed in order to obtain segmentation of the signal into cycles (Fig. 1A). This segmentation procedure, when applied to the S_{10} signal, allowed us to determine the maximal amplitude value for each cycle. In each individual neurogram, when ranked, these maximal amplitude values constituted a monotonic increasing function with an abrupt increase that revealed the threshold between buccal and lung bursts (Inset 1 in Fig. 1B). This threshold is specific to each neurogram. When the two burst populations of a neurogram (buccal and lung) were separated according to the amplitude threshold, the resulting bimodal amplitude distribution could be represented with two colors: blue for the lowest values and green for the highest ones (Inset 2 in Fig. 1B). We therefore represented the S_{10} signal as follows: identified buccal bursts appear in blue and lung bursts appear in green (Fig. 1B). Pseudo S_{200} (black) and S_{10} signals were then built separately for the buccal activity (blue) and the lung activity (green) of a given neurogram (Fig. 1C, left and right panels, respectively).

2.2.2. Burst amplitude analysis of the buccal and lung activities

The amplitude analysis was based on the building of an amplitude matrix, where (after segmentation) all the cycles of a given neurogram were stacked, aligned and ranked. This process is described in Fig. 2. Firstly, a reference cycle was defined as the cycle whose mean correlation with all the other cycles of the S_{10} signal was maximal; i.e. it was the most representative cycle of the signal of the given neurogram. Fig. 2 illustrates the process applied to a small portion of a typical S_{10} signal. In Fig. 2A a1, cycle 5 (in red) was identified as the reference cycle for the portion of the S_{10} signal represented in black (left panel). The amplitude of each cycle can be drawn as a function of time, along the y axis, or coded in shades of blue as shown for the reference cycle in Fig. 2A a2. The coded amplitudes of all the cycles were then stacked in a matrix, whose image (or 'map') is shown in Fig. 2B b1. Then, each cycle was aligned according to the time shift corresponding to the maximal value of the cross-correlation function between the cycle and the reference cycle, leading to a new matrix of the stacked cycles represented in Fig. 2B b2. In the next step, the cycles were ranked according to their maximal amplitude value, with the highest amplitudes appearing at the top. Regions of highest amplitudes (dark blue) form columns mainly in the central upper part of the map and are marked by vertical lines in Fig. 2B b3. Fig. 2C shows the mean amplitude profiles computed for each amplitude matrix represented in Fig. 2B, constructed by averaging all the amplitude values in each column (i.e. time step) of the matrix. Only the profiles of Fig. 2C c2 and c3, calculated from matrices built with the adapted temporal shifts obtained by cross-correlation with the reference cycle, exhibited amplitude peaks, whose positions corresponded to the regions of highest amplitudes appearing as dark blue columns in Fig. 2B b3 (also indicated with vertical black lines in the figure). The profiles of the aligned matrices, ranked (c3) or unranked (c2), are identical since the sorting process does not affect the time position of the cycles. In Fig. 2C c3, the amplitude profile is shown on a reduced time scale for better resolution of the burst peaks. A filtered version of this profile (yellow line in Fig. 2C c3) was computed using a zero-phase, amplitude maintaining Savitzky-Golay filter with a polynomial function of degree 3 and a moving window of 201 points (i.e. 0.1 sec). The filtered profile was then subtracted from the amplitude profile, resulting in an 'oscillation profile' (thick blue line in Fig. 2C c3) that exhibited the high frequency components only. In this way, oscillation profiles were individually computed for each neurogram. In order to evaluate how much a single oscillation prole was representative of the whole buccal burst population of a given neurogram, two oscillation proles were computed from equal numbers of buccal bursts (half the total number) randomly selected from within the neurogram. The cross-correlation coefficient, defined as the maximal value of the cross-correlation function obtained from the two buccal oscillation profiles, was computed to indicate the degree of similarity between the two oscillation profiles. This cross-correlation coefficient was termed the intra-individual cross-correlation coefficient. We also computed a cross-correlation coefficient between the respective buccal oscillation profiles characterising the neurograms from two different animals, which we term the inter-individual cross-correlation coefficient. Similarly, we calculated the lung-buccal cross-correlation coefficient to evaluate the similarity between the lung and buccal oscillation profiles within a given neurogram.

2.2.3. Frequency analysis of the separated buccal and lung activities of each neurogram

A CWT analysis was carried out on the buccal-S_{200} and lung-S_{200} signals in order to compute the corresponding time-frequency maps and to obtain frequency profiles in the range of 0.1-4 Hz, as described in Quenet et al. (2014),

i.e. a frequency profile per neurogram. Fig. 3 illustrates the principle of this time-frequency analysis. Using the S_{200} signal, amplitude values were computed for a given point (defined by a time position t and a frequency position ν) as the convolution product of the S_{200} signal, with the conjugate of a complex Morlet wavelet centered at t and of frequency ν. Time-frequency maps were then built point-by-point. Fig. 3A shows examples of Morlet wavelets with three different frequency values, placed in three different time positions relative to a buccal S_{200} signal. Each amplitude value, calculated from the S_{200} signal, was coded in gray scale: the higher the amplitude, the darker the shade. Fig. 3B shows the time-frequency map corresponding to the signal in Fig. 3A; the red star marks a dark region of the map, indicating a strong correspondence between the S_{200} signal and the wavelet shape at this time position and for this frequency, as can be seen for the red wavelet in Fig. 3A. The yellow star, corresponding to the yellow wavelet in Fig. 3A, appears on an area of the map defined by light gray shading, which indicates a poor correspondence between the wavelet shape and the signal. The time-frequency map can be represented in a 'vertical position' by interchanging the time and frequency axes, as shown in Fig. 3C. Based on these maps, a frequency profile for a given neurogram was computed by averaging data across all time points for each frequency step. In the frequency profile, shown as a blue line superimposed on the map, there was a major peak defining the fundamental frequency of the buccal rhythm. A smaller peak occurs at twice the value of the fundamental frequency and defines the second harmonic of this rhythm; the green wavelet frequency of Fig. 3A corresponds precisely to this value.

3. Results

3.1. Amplitude maps profiles of buccal bursts

As a first step, we analysed the amplitude map profiles of buccal bursts recorded from *L. catesbeianus* in order to compare them with those of *P. ridibundus*. In a previous study by Quenet et al. (2014), a temporal grid of approximately 25 Hz was found to characterise the buccal bursts recorded from CN VII of pre- and post-metamorphic *P. ridibundus*. Similar results were obtained from analysis of buccal bursts on CN V in the same species, using pre- and post-metamorphic animals (unpublished). Using *L. catesbeianus* pre- and post-metamorphic tadpoles and adults, we analysed neurograms recorded during baseline, hypoxia and hypercapnia in order to examine the amplitude map profiles across developmental stages and at levels of higher respiratory drive. Typical examples of successive buccal bursts are illustrated in Fig. 4A, and show the evolution of the buccal burst shape with advancing developmental stage: the burst activity was concentrated into a narrower time window within the buccal cycle of adults. These developmental changes were also visible in the corresponding maps (Fig. 4B) and profiles (Fig. 4C) computed for all the cycles of the buccal S_{10} signals. Similarly, the number of columns demarcated by dark blue in the computed amplitude maps (showing the areas of highest amplitude) were less numerous with development (Fig. 4B). As a consequence, this was also true for the number of peaks occurring for the mean amplitude profiles (Fig. 4C) and oscillation profiles. When the S_{10} signals recorded during hypoxia and hypercapnia were analysed, dark columns appeared within the amplitude maps and were associated with high amplitude peaks of the mean buccal profiles. The time between the oscillation profile peaks (and the dark columns of the amplitude maps), varied in the range of 30-70 ms, suggesting that the neural processes at the origin of the buccal burst temporal grid operate at a frequency of approximately 15-35 Hz. Fig. 5 illustrates the buccal amplitude map and the amplitude and oscillation profiles of six pre-metamorphic tadpoles, with two examples at stages VI, X and XII, with the intra-individual cross-correlation coefficient value indicated for each neurogram. These six values are in the range of 0.77 to 0.85. They can be compared to the values of the fifteen inter-individual cross-correlation coefficients computed from the pairs of these six neurograms, which are in the range of 0.21 to 0.39 (see the matrix of the inter-individual cross-correlation values (Fig. 6). The major difference between intra- and inter- coefficient values indicates that each neurogram is characterized by its own buccal oscillation profile, which differs significantly from the other profiles.

3.2. Variability of the lung activity

As a second step, we aimed to characterise these lung bursts using the same tools as applied to the buccal bursts. Lung activity increases with developmental stage, a trend that has been well described (for example, Taylor et al. (2003a,b)). While some lung bursting was observed in most preparations derived from pre-metamorphic tadpoles, we limited our analyses of lung activity and buccal-lung correlations to post-metamorphic tadpoles and adult frogs in order to ensure a sufficient number of lung bursts. In this regard, we only selected neurograms in which lung

bursts comprised at least 10% of the total number of respiratory bursts, with a signicant number of bursts in both populations. Based on these criteria, we selected 8 neurograms for analysis: two post-metamorphic tadpole and two adult preparations, in control (or baseline) and stimulated conditions (hypoxia for tadpoles and hypercapnia for adults). The percentage of bursts that were identified as lung ranged between 12% (Tad 2 in hypoxia) and 57% (Adult 2 in hypercapnia); the minimum number of lung bursts analysed was 32, and the minimal number of buccal bursts was 103. The left part of Fig.7 illustrates 150 sec of each of the eight S_{10} signals, with the buccal bursts shown in blue and the lung bursts in green. These signals exhibited alternations of buccal and lung activities of different durations. Note that the ratio between the lung burst amplitude and the buccal burst amplitude increased from the post-metamorphic stage to the adult stage. In the right part of Fig. 7, sections of the S_{10} signals are displayed on a reduced time scale (25 sec). In these expanded traces, different patterns of alternation of buccal and lung bursts were clearly visible, where lung episodes were in the form of lung 'clusters' (i.e. the lung bursts were not separated by buccal bursts) or groups of isolated bursts (i.e. the lung bursts were separated by at least one buccal burst). The buccal/lung alternation configuration was variable within an individual neurogram; in Fig. 7 for example, the activity of Tadpole 2 changes from isolated bursting to a cluster around 90 sec during the hypoxic condition. Regardless of whether the lung bursts occurred in clusters or as isolated bursts, lung bursts for a given S_{10} signal emerged on a low-frequency time grid that was similar to the time grid that dened the buccal burst rhythm.

3.3. Frequency profiles

We analysed the separated buccal S_{200} and lung S_{200} signals for each preparation with CWT. Fig. 8 presents low-frequency (0.1-4 Hz) time-frequency maps and the corresponding frequency profiles of these signals. Each background map is composed of the buccal map in the lower part and the lung map in the upper part, with the horizontal threshold between buccal and lung indicated by a dashed red line. The y-axis time scale corresponds to the cumulated time of both maps. Maps and profiles are associated in vertical pairs for each of the four preparations recorded during two conditions (Fig. 8A, baseline; Fig. 8B, stimulated condition). All the frequency profiles, from both buccal and lung signals, showed a dominant peak around approximately 1 Hz. Depending on the preparation, the maximum ranged between 0.7 to 1.3 Hz. For each preparation in a given condition, buccal and lung dominant peaks were near-coincident: in 5 of the 8 recordings the frequency difference between the buccal and the lung dominant frequency was less than or equal to the frequency precision of the CWT, i.e. the step increment of 0.1 Hz. For the other three recordings, the difference was twice or three times this value (see Fig. 8A: Tad 1; Fig. 8B Tad 1, Adult 1).

3.4. Amplitude maps, amplitude and oscillation profiles of lung and buccal bursts

For the 8 selected S_{10} signals, we analysed the temporal grid inside the lung and buccal bursts and compared them to each other: first within the same neurograms and then between neurograms of the same preparation (i.e. we compared baseline with the stimulated condition). The results of the lung burst analysis, performed using the same processing tools applied to the buccal bursts, are presented in Fig. 9. Data for the 4 buccal and lung S_{10} signals are presented in vertical pairs (Fig. 9A, baseline; Fig. 9B, stimulated condition). The same reference cycle (the cycle most correlated with all the buccal and lung bursts in the baseline condition) was used for the alignment process of the cycles recorded from a given preparation (Tad1, Tad 2, Adult 1 Adult 2). The mean amplitude profiles, oscillation profiles and amplitude maps are shown in green for lung cycles (Fig. 9A1, A2; B1, B2) and in blue for buccal cycles (Fig. 9A3, A4; B3, B4). Dark blue columns marking areas of highest amplitude were observed in the buccal amplitude maps for all developmental stages and in all conditions (Fig. 9A3 and B3). Columns were systematically prolonged in the lung amplitude maps (appearing as dark green columns in Fig. 9A2 and B2), corresponding to approximately the same time range as observed for the dark blue columns of the buccal amplitude maps. These findings indicated that the lung bursts were also temporally organised according to the same temporal grid as that of the buccal bursts, for each neurogram. This temporal grid was also clearly visible when comparing the buccal and lung amplitude profiles and oscillation profiles, since they exhibit similar peak positions for a given neurogram. The degree of similarity between lung and buccal oscillation proles was quantied by the lung-buccal cross-correlation coefficient (red text in Fig. 9) computed for each neurogram. Coefficient values ranged between 0.67 to 0.89, where a value of '1' would indicate a perfect match between the profiles. Intra-individual cross-correlation coefficient values for buccal activity are shown for each neurogram in Fig. 9 (blue text). These values ranged from 0.77 to 0.91, and were therefore similar to the coefficient values obtained for the lung-buccal cross-correlation analysis. The intra-individual cross-correlation coefficient values can be compared to the two inter-individual coefficients values, the latter having been

Table 1. Correlation coefficients between oscillation profiles in baseline and stimulated conditions

Tadpoles				
Preparation		baseline/hypoxia		
Tadpole 1	Buccal	0.93	Lung	0.78
Tadpole 2	Buccal	0.95	Lung	0.75
Adults				
Preparation		baseline/hypercapnia		
Adult 1	Buccal	0.92	Lung	0.58
Adult 2	Buccal	0.86	Lung	0.85

calculated using buccal oscillation profiles from two tadpoles (Tad 1/Tad 2) and two adult frogs (Adult 1/Adult 2) during baseline conditions. The inter-individual cross-correlation coefficient values for post-metamorphic tadpoles and adult frogs were 0.38 and 0.32, respectively. Since the intra-individual correlation values exceeded the inter-individual correlation values, it indicates that buccal oscillation profiles were more correlated within a preparation than between preparations and that (as with the pre-metamorphic tadpoles) the buccal oscillation proles appeared specic for each neurogram. Moreover, each lung oscillation prole was very similar to the corresponding buccal oscillation prole. Table 1 summarises the cross-correlation coefficients for the comparison between baseline and stimulated conditions for the buccal and lung oscillation proles of each preparation.

4. Discussion

In this work, we analysed filtered neurograms exhibiting ventilatory motor rhythms similar to those recorded in intact *L. catesbeianus* (Vasilakos et al. (2004), Santin & Hartzler (2016)). The first main conclusion of our results is that, regardless of the developmental stage or conditions (baseline, hypoxia or hypercapnia), all the buccal bursts of a given neurogram exhibited a temporal grid, which specific to that neurogram. This is evidence by the high value of the buccal intra-individual cross-correlation coefficients, when compared to the buccal inter-individual cross-correlation coefficients. This temporal grid observed in *L. catesbeianus* is reminiscent of the temporal grid also observed for the buccal bursts of *P. ridibundus* (Quenet et al. (2014)). Our second main conclusion stems from the cross-correlation analysis applied to the lung bursts of post-metamorphic tadpoles and adults, which reveals the presence of the same temporal grid for lung bursts and buccal bursts, with lung-buccal cross-correlation coefficient values that are in the same range as the buccal intra-individual cross-correlation coefficients. The third important conclusion relates to the frequency profiles computed using CWT applied separately to the reconstructed buccal and lung signals in post-metamorphic and adult frogs: both signals exhibit the same fundamental frequency at approximately 1 Hz, whatever the alternation pattern. This nding suggests that a clock provides the same drive for both buccal and lung rhythms and that this clock has specic properties for each animal. Previous studies on adult frogs also describe a time frame for buccal and lung activities, using histograms (Vasilakos et al. (2004)) or Poincare plots (Vasilakos et al. (2004), Fong et al. (2009)) with a time unit corresponding to the minimum buccal burst interval (Vasilakos et al. (2004)) or the minimum lung burst interval (Fong et al. (2009)). A common drive for both buccal and lung activities was also assumed by Milsom (2010) to explain the common time frame on which buccal and lung activities seem to be organised. This fundamental low-frequency organisation defines a slow time scale of muscle activation: that of the buccal floor movement, with small amplitudes for buccal ventilation and higher amplitudes for lung ventilation. The high-frequency temporal grid apparent within both buccal and lung bursts defines another time scale that we propose to be a characteristic of the ventilatory CPG. Indeed, the motoneuronal activities recorded in neurograms are driven by this CPG, with several synaptic transmission steps that introduce stochastic noise effectively blurring the original time organisation of the central command. This neuronal noise is an intrinsic feature of motor control that limits direct analysis of CPG dynamic properties. Our analysis, based on the computation of mean amplitude and oscillation

profiles of a neurogram, aims to retain information on features that are time invariant, burst after burst, therefore reducing the blurring effect of noise.

The relevance of the results obtained from this amplitude analysis depends on the number of bursts analysed, and it was for this reason that we only retained neurograms for the analysis of lung activity which had a sufficient number of lung bursts. Although our results are limited to some extent by the use of a relatively few animals, we ensured sufficient sampling of bursts within the selected neurograms. As a consequence, our present analysis deals with burst-specific features in each preparation. For each neurogram, the cross-correlation analysis between the lung and buccal oscillation profiles indicates that they are very similar; this indicates that the buccal and lung bursts share the same temporal grid. These results suggest a dynamic coupling between the buccal and lung oscillators, major components of the ventilatory CPG. In addition, the cross-correlation coefficients listed in Table 1 for the buccal oscillation profiles during baseline vs. stimulated conditions indicate that the temporal grid is not significantly affected by hypoxia or hypercapnia in our preparations. Similarly, the cross-correlation coefficients computed for the lung oscillation proles were high, but were smaller than the buccal coefficients; this is likely a consequence of the smaller number of lung bursts analysed resulting in computed oscillation proles that were more noisy than those for the buccal activities. Our interpretation of the temporal grid observed within the buccal bursts of both *L. catesbeianus* and *P. ridibundus* relies on measurements done using the unfiltered neurograms presented in Fig. 6 and Fig. 7 of Quenet et al. (2014) for pre- and post-metamorphic tadpoles, respectively. In this study, the peak amplitude value of a buccal burst amplitude profile corresponded to the numerous high peaks in the neurograms, within the same time window. These neurogram peaks result from the sum of synchronised firings of individual motoneurons within a time window of about 20 ms. Such a synchronisation process occurs in *P. ridibundus* approximately every 40 ms, corresponding to the 25 Hz process proposed to be at the origin of this temporal grid. In Horcholle-Bossavit & Quenet (2019), synchronising mechanisms in the ventilatory CPG are proposed to account for the presence of the temporal grid within the buccal bursts; these CPG mechanisms were validated by simulations of neurograms exhibiting the same dynamic features as those of the experimental recordings. In *L. catesbeianus* neurograms, we suggest that the same type of synchronisation process occurs at the level of the motoneurons, with a similar temporal grid and time lags between two synchronisations that vary from 30 to 70 ms. The high- and low-frequency features that are common to both the buccal and lung bursts recorded from the same preparation suggest a relationship between these two rhythms.

The question that arises is how the coupling process between the buccal and the lung activities is established. The hypothesis that there are two separate respiratory oscillators, one in a rostral location for the lung command and the other one in caudal location for the buccal command, is supported by previous studies (see Reed et al. (2018)). In addition, data from a recent study suggests that a third oscillator, termed the 'priming oscillator' may surround the region of the lung oscillator (Baghdadwala et al. (2015)). This recently identified oscillator is thought to be responsible for the 'priming activity' that precedes the high amplitude peak of lung bursts, and is visible on the integrated CN VII and spinal nerve II neurograms, but quasi-inexistent on CN V and X neurograms. Since our analyses focused on CN V neurograms only, our data cannot provide information about the possible participation of this new oscillator in the observed coupling mechanisms. The important question of the nature of coupling between the lung and buccal oscillators was considered in two recent studies. In (Trask et al. (2018)), this coupling was specifically evaluated by the lung-buccal offset time; i.e. the peak-to-peak time interval between a lung burst and the previous buccal burst. The coefficient of variation of this descriptor was used as a measurement of the coupling strength between the two rhythms. The results of Trask et al. show a decrease in the value of this coefficient with development, indicating that as metamorphosis advances the rhythms produced by the buccal and lung oscillators become more tightly coordinated. In the study of (Reed et al. (2018)), the authors performed transverse sections at several levels in the isolated brainstems of *L. catesbeianus* in order to assess areas critical for lung rhythmogenesis and chemosensitivity. The removal of caudal structures in these preparations stimulated the frequency of lung ventilatory bursts and revealed a hypercapnic response in normally unresponsive preparations derived from early-staged tadpoles(TK: IV-IX). In late-staged tadpoles (TK: XIX-XXIV) however, removal of caudal brainstem structures reduced the lung burst frequency and hypercapnic responsiveness was retained. These results seem to confirm the hypothesis that inhibition of lung motor activity in early-staged tadpoles originates from the caudal medulla, and possibly from the region of the buccal oscillator where GABAergic and glycinergic mechanisms have been investigated. However, the inhibitory influence of the caudal medullary sites appears to change as metamorphosis progresses (Galante et al. (1996), Straus et al. (2000), Broch et al. (2002), Vasilakos et al. (2006), Leclere et al. (2012)). These studies suggest that the expression of lung activity is only inhibited by the caudal medulla during early development, and that this inhibition is gradually

reduced as metamorphosis progresses; and possibly replaced by excitatory connections.

In our study, the neurograms from pre-metamorphic tadpoles also exhibit a very low occurence of lung activity, which precluded a significant analysis of the lung burst features in this stage group. Therefore, we cannot evaluate any coupling between the lung and buccal oscillators in this stage group. For the post-metamorphic tadpoles and adults exhibiting a sufficient number of lung bursts in each neurogram, the cross-correlation coefficients indicated a comparable level of coupling in the adult frogs and in post-metamorphic tadpoles. The buccal-lung dynamic coupling could involve buccal-lung oscillator connections, in combination with structures in the brainstem medulla providing additional drive. In the work of Reed et al. (2018), such structures are presented as independent transverse layers, one located rostral to the lung oscillator and driving its activity, and another located between the lung and the buccal oscillator driving activity of the buccal oscillator. According to this configuration, a transverse section isolating the two oscillators maintains their specific inputs and their respective rhythms. The same experimental observations could also be explained by an anatomical alternative, where a unique structure providing drive to the respiratory oscillators has a rostro-caudal organisation, and whose rostral region may project onto the lung oscillator, while the caudal region projects onto the buccal oscillator. This structure providing a common drive could be a good candidate to explain both (1) the common dynamic features of the lung and buccal rhythms in intact preparations, and (2) the persistence of the two rhythmic activities when the two oscillators are separated. Taking into account all the results of these recent studies, a specific ventilatory CPG model integrating these data should be built in order to simulate neurograms with the dynamic features of those recorded in *L. catesbeianus*.

References

Baghdadwala, M. I., Duchcherer, M., Paramonov, J., & Wilson, R. J. A. (2015). Three brainstem areas involved in respiratory rhythm generation in bullfrogs. *J. Physiol.*, *593(13)*, 29412954.

Broch, L., Morales, R. D., Sandoval, A. V., & Hedrick, M. S. (2002). Regulation of the respiratory central pattern generator by chloride-dependent inhibition during development in the bullfrog (rana catesbeiana). *J. Exp. Biol.*, *205*, 11611169.

Burggren, W., & West, W. (1982). Changing respiratory importance of gills, lungs and skin during metamorphosis in the bullfrog rana catesbeiana. *Respir. Physiol.*, *47(2)*, 151–64.

DelNegro, C. A., Funk, G. D., & Feldman, J. L. (2018). Breathing matters. *Nat. Rev. Neurosci.*, *19(6)*, 351367.

Duchcherer, M., Baghdadwala, M. I., Paramonov, J., & Wilson, R. J. (2013). Localization of essential rhombomeres for respiratory rhythm generation in bullfrog tadpoles using a binary search algorithm: Rhombomere 7 is essential for the gill rhythm and suppresses lung bursts before metamorphosis. *Dev. Neurobiol.*, *73(12)*, 888–98.

Feldman, J. L., & DelNegro, C. A. (2006). Looking for inspiration: New perspectives on respiratory rhythm. *Nature Reviews Neuroscience*, *7*, 232242.

Fong, W. Y., Zimmer, M. B., & Milsom, W. K. (2009). The conditional nature of the "central rhythm generator" and the production of episodic breathing. *Respir. Physiol. Neurobiol.*, *168 (1-2)*, 179–87.

Fournier, S., Allard, M., Roussin, S., & Kinkead, R. (2007). Developmental changes in central o2 chemoreflex in rana catesbeiana: the role of noradrenergic modulation. *J. Exp. Biol.*, *210*, 3015–26.

Galante, R. J., Kubin, L., Fishman, A. P., & Pack, A. I. (1996). Role of chloride-mediated inhibition in respiratory rhythmogenesis in an in vitro brainstem of tadpole, rana catesbeiana. *J. Physiol.*, *492*, 545–558.

Gans, C., de Jongh, H. J., & Farber, J. (1969). Bullfrog (rana catesbaiana) ventilation: how does the frog breathe? *Science*, *163(3872)*, 1223–5.

Gdovin, M. J., Torgerson, C. S., & Remmers, J. E. (1998). Neurorespiratory pattern of gill and lung ventilation in the decerebrate spontaneously breathing tadpole. *Respir. Physiol.*, *113*, 135–146.

Gdovin, M. J., Torgerson, C. S., & Remmers, J. E. (1999). The fictively breathing tadpole brainstem preparation as a model for the development of respiratory pattern generation and central chemoreception. *Comp. Biochem. Physiol. A Mol. Integr. Physiol.*, *124*, 275–286.

Horcholle-Bossavit, G., & Quenet, B. (2019). Neural network model of an amphibian ventilatory central pattern generator. *J. Comput. Neurosci.*, *46*, 1–22.

Jones, R. M. (1982). How toads breathe: control of air flow to and from the lungs by the nares in bufo marinus. *Respir. Physiol.*, *49(2)*, 25165.

Kogo, N., Perry, S. F., & Remmers, J. E. (1994). Neural organization of the ventilatory activity in the frog, rana catesbeiana. *Journal of Neurobiology*, *25*, 10671079.

Kogo, N., & Remmers, J. E. (1994). Neural organization of the ventilatory activity in the frog, rana catesbeiana. *Journal of Neurobiology*, *25*, 10801094.

Leclere, R., Straus, C., Similowski, T., Bodineau, L., & Fiamma, M. N. (2012). Persistent lung oscillator response to co2 after buccal oscillator inhibition in the adult frog. *Respir. Physiol. Neurobiol.*, *183*, 166–169.

Maclntyre, D. H., & Toews, D. P. (1976). The mechanics of lung ventilation and the effects of hypercapnia on respiration in bufo marinus. *Can. J. Zool.*, *54*, 13641373.

McLean, H. A., Kimura, N., Kogo, N., Perry, S. F., & Remmers, J. E. (1995). Fictive respiratory rhythm in the isolated brainstem of frogs. *J. Comp. Physiol. A*, *176*, 703–713.

Milsom, W. K. (2010). Adaptive trends in respiratory control: a comparative perspective. *Am. J. Physiol. Regul. Integr. Comp. Physiol.*, *299(1)*, R1–10.

Oku, Y., Kimurab, N., Masumiyaa, H., & Okadac, Y. (2008). Spatiotemporal organization of frog respiratory neurons visualized on the ventral medullary surface. *Resp. Phys. and Neurobiol.*, *161*, 281–290.

Onimaru, H., & Homma, I. (2003). A novel functional neuron group for respiratory rhythm generation in the ventral medulla. *J. Neurosci.*, *23(4)*, 1478–86.

Quenet, B., Straus, C., Fiamma, M. N., Rivals, I., Similowski, T., & Horcholle-Bossavit, G. (2014). New insights in gill/buccal rhythm spiking activity and co_2 sensitivity in pre- and post-metamorphic tadpoles *pelophylax ridibundus*. *Resp. Physiol. and Neurobiol.*, *191*, 26–37.

Reed, M. D., Iceman, K. E., Harris, M. B., & Taylor, B. E. (2018). The rostral medulla of bullfrog tadpoles contains critical lung rhythmogenic and chemosensitive regions across metamorphosis. *Comp. Biochem. Physiol. A Mol. Integr. Physiol.*, *225*, 715.

Sakakibara, Y. (1984a). The pattern of respiratory nerve activity in the bullfrog. *Jpn. J. Physiol.*, *34*, 269–282.

Sakakibara, Y. (1984b). Trigeminal nerve activity and buccal pressure as an index of total inspiratory activity in the bullfrog. *Jpn. J. Physiol.*, *34*, 827–838.

Santin, J. M., & Hartzler, L. (2016). Reassessment of chemical control of breathing in undisturbed bullfrogs, lithobates catesbeianus, using measurements of pulmonary ventilation. *Resp. Physiol. and Neurobiol.*, *224*, 80–89.

Smith, J. C., Ellenberger, H. H., Ballanyi, K., Richter, D. W., & Feldman, J. L. (1991). Pre-botzinger complex: A brainstem region that may generate respiratory rhythm in mammals. *Science*, *254*, 726–729.

Straus, C., Wilson, R. J., Montcel, S. T. D., & Remmers, J. E. (2000). Baclofen eliminates cluster lung breathing of the tadpole brainstem, in vitro. *Neurosci. Lett.*, *292*, 1316.

Sundin, L., Burleson, M. L., Sanchez, A. P., Amin-Naves, J., Kinkead, R., Gargaglioni, L. H., Hartzler, L. K., Wiemann, M., Kumar, P., & Glass, M. L. (2007). Respiratory chemoreceptor function in vertebratescomparative and evolutionary aspects. *Integrative and Comparative Biology*, *47(4)*, 592600.

Taylor, B. E., Harris, M. B., Leiter, J. C., & Gdovin, M. J. (2003a). Chemoreception in developing bullfrogs: anomalous response to acetazolamide. *J. Appl. Physiol (1985)*, *94*, 12041212.

Taylor, B. E., Harris, M. B., Leiter, J. C., & Gdovin, M. J. (2003b). Ontogeny of central co2 chemoreception: chemosensitivity in the ventral medulla of developing bullfrogs. *Am. J. Phys. Regul. Integr. Comp. Phys.*, *285*, R1461R1472.

Torgerson, C. S., Gdovin, M. J., & Remmers, J. E. (1997). The ontogeny of central chemoreception during fictive gill and lung ventilation of an in vitro brainstem preparation of rana catesbeiana. *J. Exp. Biol.*, *299*, 2063–2072.

Trask, W. M., Baghdadwala, M. I., & Wilson, R. J. (2018). Developmental maturation of functional coupling between ventilatory oscillators in the american bullfrog. *Dev. Neurobiol.*, *78(12)*, 1218–1230.

Vasilakos, A., Wilson, R. J., Kimura, N., & Remmers, J. E. (2004). Ancient gill and lung oscillators may generate the respiratory rhythm of frogs and rats. *J. Neurobiol.*, *62*, 369–385.

Vasilakos, K., Kimura, N., .Wilson, R. J., & Remmers, J. E. (2006). Lung and buccal ventilation in the frog: uncoupling coupled oscillators. *Physiol. Biochem. Zool.*, *79*, 1010–8.

Vitalis, Z., & Shelton, G. (1990). Breathing in rana pipiens: The mechanisms of ventilation. *J. exp. Biol.*, *154*, 537–556.

West, N. H., & Jones, D. R. (1975a). Breathing movements in the frog rana pipiens. i. the mechanical events associated with lung and buccal ventilation. *Can. J. Zool.*, *53(3)*, 332344.

West, N. H., & Jones, D. R. (1975b). Breathing movements in the frog rana pipiens. ii. the power output and efficiency of breathing. *Can. J. Zool.*, *53(3)*, 345353.

Wilson, R. J. A., Straus, C., & Remmers, J. E. (1999). Efficacy of a low volume recirculating superfusion chamber for long term administration of expensive drugs and dyes. *J. Neurosci. Methods*, *87*, 175–184.

Wilson, R. J. A., Vasilakos, K., Harris, M., Straus, C., & Remmers, J. (2002). Evidence that ventilatory rhythmogenesis in the frog involves two distinct neuronal oscillators. *J. Physiol.*, *557-570*, 545–558.

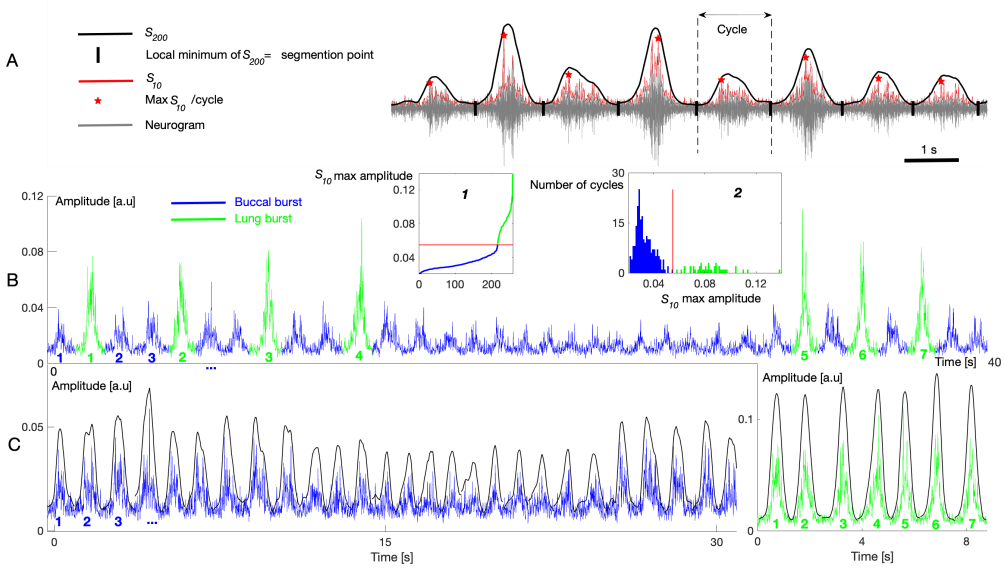

Figure 1. Separation of the buccal and lung bursts, and building of the buccal and lung signals. A) A neurogram recorded from a post-metamorphic tadpole is shown in gray. A filtered S_{200} signal (in black) is superimposed on the neurogram and shows minima (small black rectangles) that correspond to the segmentation points delimiting each buccal or lung burst cycle. A second filtered signal, the S_{10} signal (in red), is also superimposed on the neurogram; the maximal amplitude of each burst is labeled by a red star. B) Inset 1 shows a plot of the ranked amplitude values of the maximal amplitude for all buccal (blue) and lung (green) bursts; the red horizontal line indicates the threshold which separates the buccal and lung amplitudes. The histogram shown in inset 2 plots the maximal amplitudes per burst revealing a bimodal pattern corresponding to the two burst populations; the vertical red line separates the buccal burst population (in blue) from the lung burst population (in green). The S_{10} signal depicts the respiratory bursts after separation into 'buccal' (blue) and 'lung' (green). Lung bursts are numbered 1-7 for clarity, and the first three buccal bursts of the signal are labeled 1-3. C) Left panel: The buccal S_{10} signal (blue) and S_{200} signal (black) are built by concatenation of all the buccal bursts ranked in their chronological order. Right panel: The lung S_{10} signal (green) and S_{200} signal (black) are built using the same procedure.

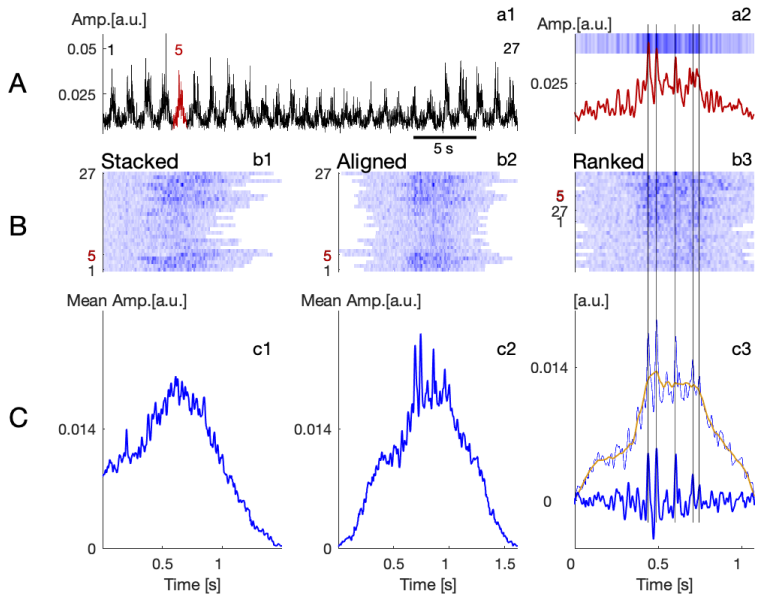

Figure 2. Building of an amplitude map and computation of the mean amplitude profile. A) a1: The Buccal S_{10} signal containing 27 bursts. Burst number 5 (in red) is the reference cycle, i.e. the cycle that is the most correlated with the other 26 bursts. a2: The amplitudes of the reference cycle are coded in shades of blue and plotted across time; darker shades correspond to higher amplitude values. B) b1: Each of the 27 buccal cycles are coded across their timespan in shades of blue according to their amplitude at a given time point. A preliminary amplitude map is created by stacking all the coded bursts by their chronological order. b2: The temporal position of each cycle is determined by the time lag where the cross-correlation function between the cycle and the reference cycle is maximal, in such a way that all the cycles are aligned with the reference cycle. b3: the cycles are then ranked according to their maximal amplitude, the smallest amplitudes are placed at the bottom of the map, and the largest are placed at the top (the timescale for this map was reduced to 1 sec). C) A mean amplitude profile is computed for each corresponding map and shown in c1, c2 and c3. When compared to profile in c1, the mean amplitude profile of c2 exhibits high amplitude oscillations. In c3, the computed mean amplitude profile (thin blue line) is exactly the same as that for c2. The profile in c3 is shown on a reduced time of 1 sec encompassing the central part of the signal. A filtered version of the mean amplitude profile is computed (shown in yellow), and subtracted from the profile: the resulting 'oscillation profile' is drawn using a thick blue line. The vertical black lines passing through a2 to c3 indicate the correspondence between the maxima of the reference burst profile, amplitude profile and oscillation profile, and the columns of dark blue on the amplitude map.

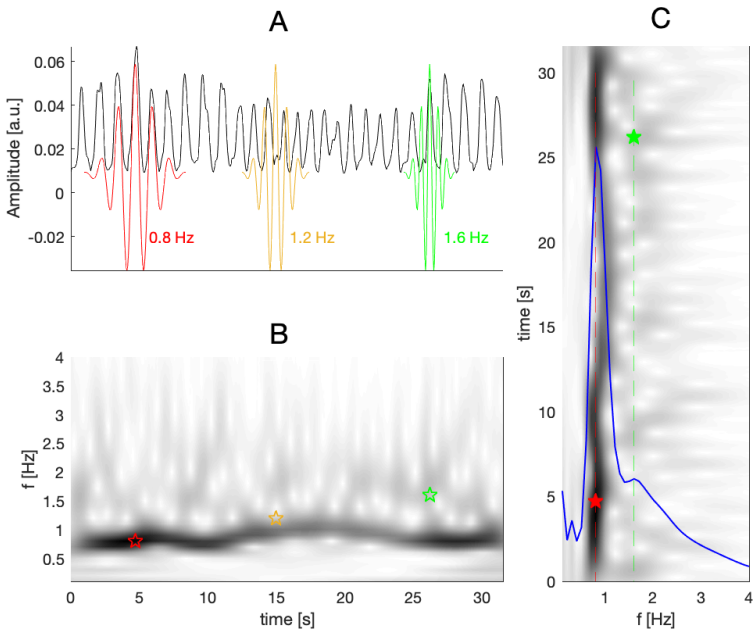

Figure 3. Computation of 1) a time-frequency CWT map using complex Morlet wavelets, and 2) the corresponding mean frequency profile. A) Illustration of three complex Morlet wavelets that differ in time position t, and frequency ν (ν =0.8 Hz in red, 1.2 Hz in yellow and 1.6 Hz in green), superimposed onto the S_{200} buccal signal shown in black. B) The amplitude values of the signal are computed by convolution of the S_{200} signal with the conjugate of the Morlet Wavelet centered at t, and of frequency ν. Values are coded in shades of gray for each point (t,ν) of the time-frequency map, where darker shades represent higher amplitudes. Each of the red, yellow and green stars indicates the (t,ν) point of one of the three corresponding wavelets illustrated in A, respectively. C) A mean frequency profile (blue) is shown superimposed on the time-frequency map with the frequency in abscissa, and reveals a peak at 0.8 Hz (red dashed line) corresponding to the fundamental frequency of the buccal rhythm. The green dashed line indicates the second harmonic frequency.

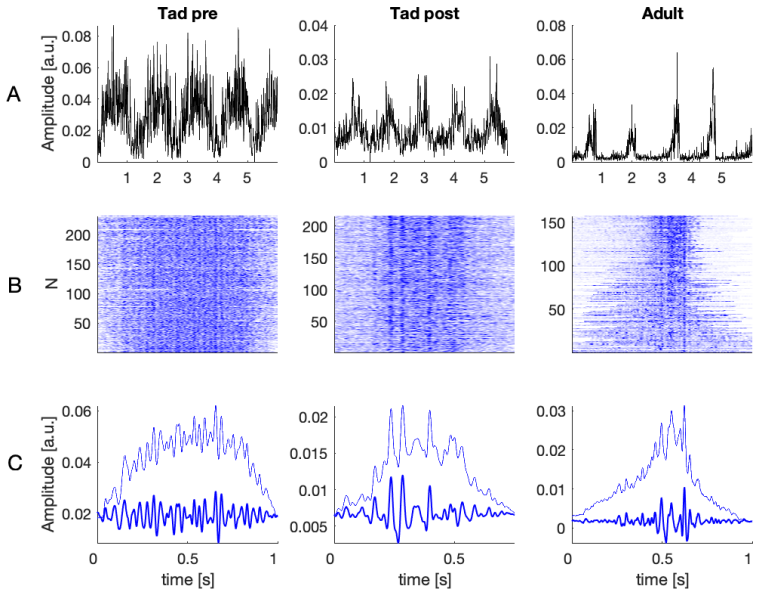

Figure 4. Examples of typical buccal amplitude maps, amplitude and oscillation profiles for different developmental stages before and after metamorphosis. A) Five sec intervals of the S_{10} signals demonstrate the buccal burst shapes in a pre-metamorphic tadpole (stage X), a post-metamorphic tadpole and an adult frog. B) Amplitude maps were built by stacking the cross-correlated aligned amplitudes of all the buccal cycles segmented in the corresponding S_{10} signal, i.e. one map per neurogram. Each panel corresponds to the signal shown above in (A). C) An amplitude profile (thin blue line) was calculated for each neurogram by averaging all the amplitudes appearing in each time column of the corresponding amplitude map, and an oscillation profile (thick blue line) was computed by subtraction of the filtered profile from each amplitude profile, as described in Fig. 2C.

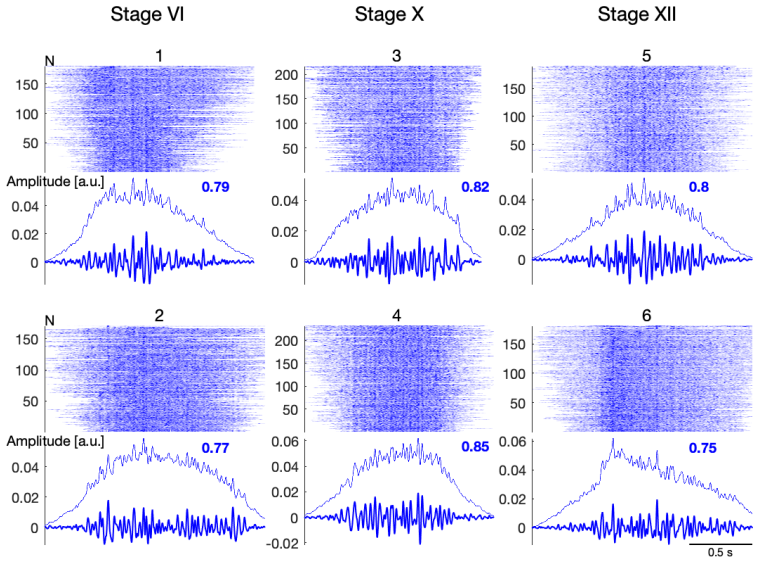

Figure 5. Amplitude maps, amplitude profiles and oscillation profiles of buccal bursts in six pre-metamorphic tadpole neurograms. Maps and profiles are shown for two preparations at stage VI (1,2), two at stage X (3,4) and two at stage XII (5,6) in baseline conditions. The intra-individual oscillation profile cross-correlation coefficient is indicated in blue (see methods).

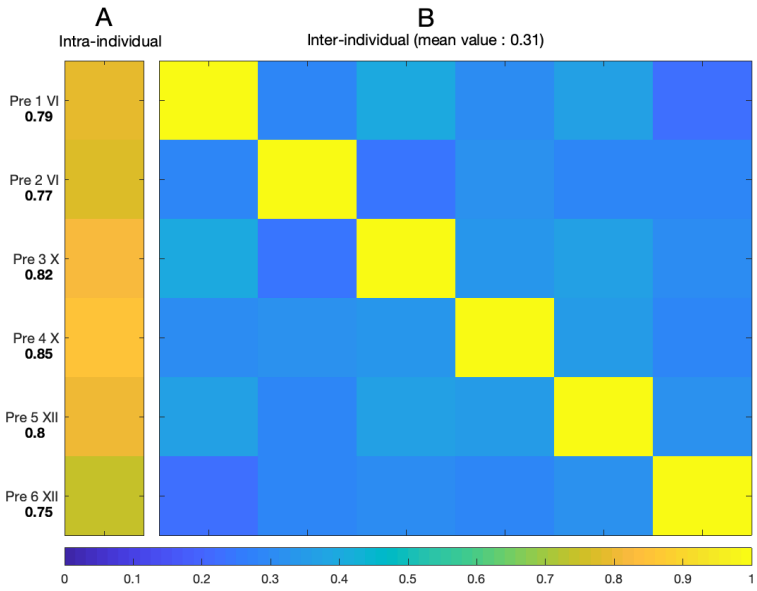

Figure 6. Intra- and inter-individual buccal cross-correlation coefficients for pre-metamorphic tadpoles. A): vector of intra-individual cross-correlation coefficients for the six pre-metamorphic tadpoles, whose amplitude and oscillation profiles are presented in Fig. 5. B): matrix of inter-individual cross-correlation coefficients for pairs of oscillation profiles for these six pre-metamorphic tadpoles (Note that the diagonal contains the coefficients for the cross-correlation of each oscillation profile with itself, all the six values are 1 by definition).

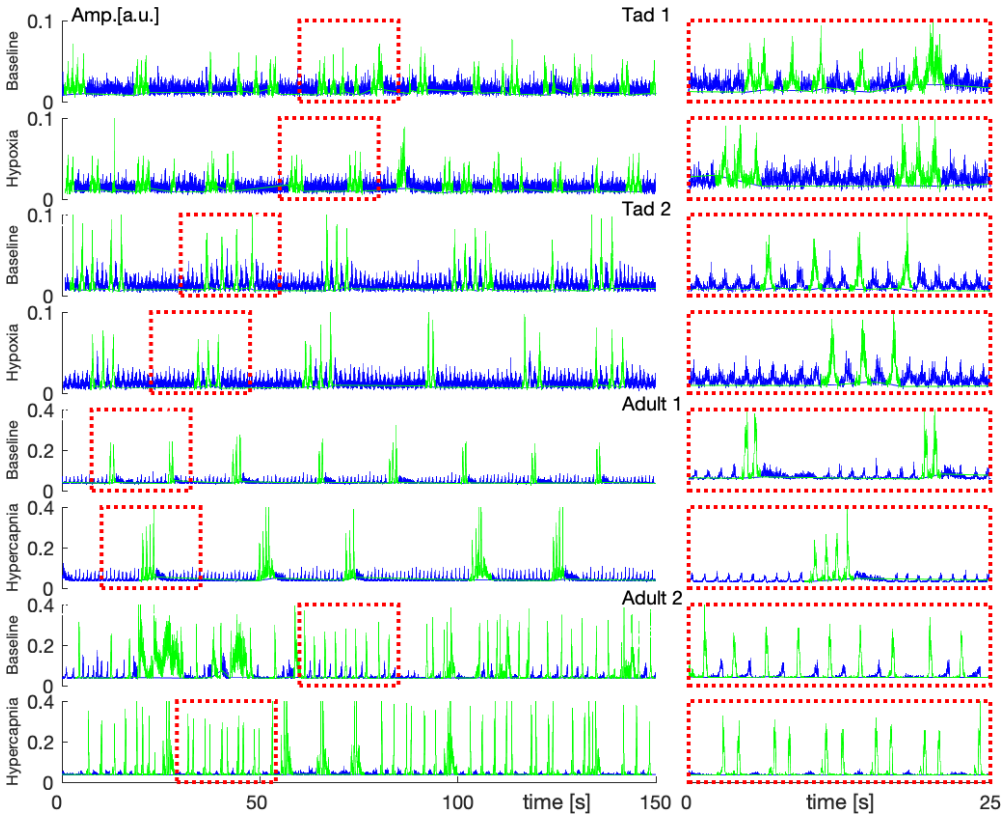

Figure 7. A set of S_{10} signals computed from post-metamorphic tadpole and adult frog neurograms exhibiting buccal and lung activities. These signals were recorded during baseline, hypoxia (post-metamorphic tadpoles) or hypercapnia (adult) conditions. The left panels illustrate 150 seconds of the signals, with the buccal bursts outlined in blue and the lung bursts outlined in green. Red dashed rectangles indicate the specific region of the signals that are represented on a reduced time scale in the right panels of the figure. The 25 sec S_{10} signals shown in the right panels demonstrate the different types of buccal/lung alternation patterns.

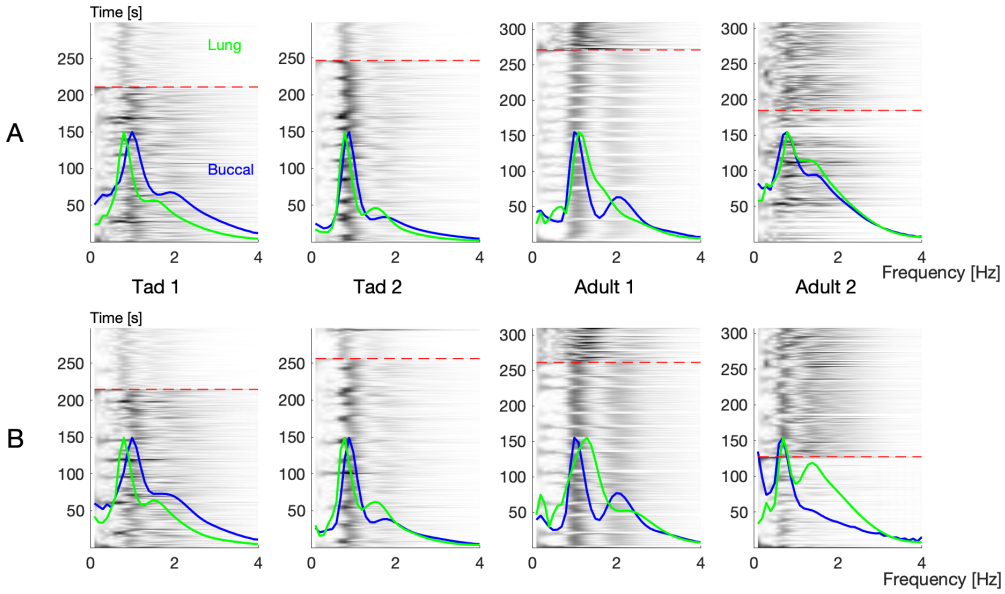

Figure 8. Time-frequency maps and frequency profiles from buccal and lung S_{200} signals for post-metamorphic tadpoles and adult frogs. The time-frequency data for the buccal signal appears on the lower part of the map and is separated from the lung data (top part of map) by the red dashed line. The time scale on the y axis corresponds to the cumulated time (in sec) for the two maps. Superimposed onto the background map are the mean frequency profiles for buccal (blue) and lung (green). The amplitudes of these two profiles have been scaled in order to normalise their respective maxima to the same amplitude value. A) Baseline. B) Hypoxia for post-metamorphic tadpoles and hypercapnia for adult frogs.

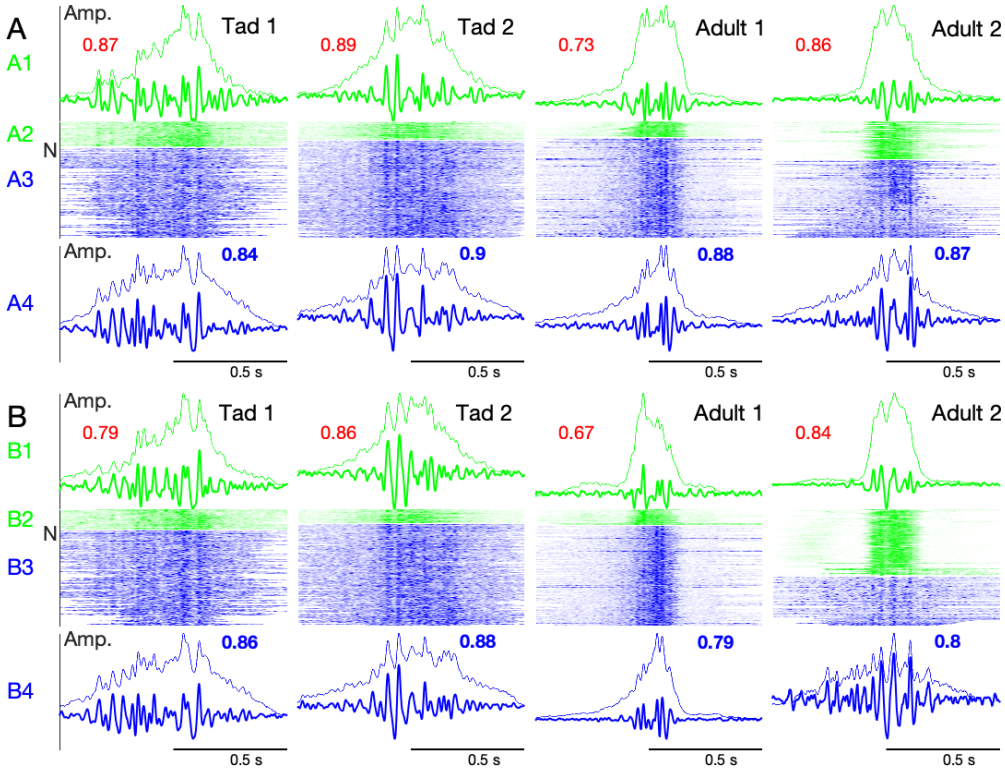

Figure 9. Amplitude maps, amplitude profiles and oscillation profiles of buccal and lung bursts computed from the S_{10} signals for post-metamorphic tadpoles (left two panels, Tad 1 and Tad 2, in baseline (A) and hypoxia (B)) and adult frogs (right two panels, Adult1 and Adult 2, in baseline (A) and hypercapnia (B)). A) Amplitude maps of the S_{10} signal during baseline are presented with the lung (green, A2) and buccal (blue, A3) cycles ranked in ascending order of their maximal amplitudes. The corresponding amplitude and oscillation profiles are shown in green (A1) for the lung bursts, and in blue (A4) for the buccal bursts. B) Amplitude maps, amplitude profiles and oscillation profiles are shown for the corresponding buccal and lung S_{10} signals during stimulated conditions: hypoxia for post-metamorphic tadpoles and hypercapnia for adult frogs. The intra-individual buccal oscillation profile cross-correlation coefficient is indicated in blue and the cross-correlation coefficient for each of the buccal-lung oscillation profile pairs is indicated as a red number above the lung profile.